Available online at www.sciencedirect.com
SCIENCE DIRECT
International Journal of Heat and Mass Transfer 49 (2006) 2663–2672
International Journal of HEAT and MASS TRANSFER
www.elsevier.com/locate/ijhmt

Correlation of critical heat flux in hybrid jet impingement/micro-channel cooling scheme

Myung Ki Sung, Issam Mudawar *

Purdue University International Electronic Cooling Alliance (PUIECA), West Lafayette, IN 47907, USA

Received 16 August 2005; received in revised form 9 January 2006
Available online 10 March 2006

Abstract

Experiments were performed to investigate the two-phase cooling characteristics of a new hybrid cooling scheme combining the cooling attributes of slot jets and micro-channel flow. A test module was constructed in which dielectric PF-5052 liquid was introduced through five 0.48 mm wide and 12.7 mm long slot jets, each leading to a 1.59 mm wide and 1.02 mm deep channel. Increases in flow rate and subcooling yielded similar trends of delaying the inception of boiling and increasing critical heat flux (CHF). A previous channel flow correlation predicted CHF values far smaller than measured, while those for slot jets yielded closer predictions. This proves the cooling performance of the hybrid configuration is dominated more by jet impingement than by micro-channel flow. By dividing the test surface into a portion that is dominated by jet impingement and another by micro-channel flow, and applying the appropriate CHF correlation for each portion, the CHF data for this hybrid cooling configuration are predicted with a mean absolute error of 8.42%.

1. Introduction

The quest for speed in modern electronic devices has led to aggressive micro-miniaturization of electronic components and insertion of an increasing number of components in a given device surface area. These advances have precipitated substantial increases in heat dissipation both at the device and systems levels. More powerful cooling systems are therefore needed to meet those challenges.

Convective cooling with phase change is especially attractive for these applications because of the enormous heat transfer coefficients that can be realized. For a given coolant temperature, such high convection coefficients facilitate the removal of large heat fluxes while maintaining relatively small device surface temperatures. Another important advantage of phase change stems from the strong dependence of the heat transfer coefficient on heat flux. Large increases in the magnitude of the heat transfer coefficient with increasing heat flux implies the device will incur only modest temperature increases corresponding to fairly substantial increases in power dissipation [1]. Minimizing the fluctuations in device temperature is paramount to both the reliability and the structural integrity of an electronic package.

However, phase change systems are not without drawbacks. They are typically more difficult to implement and more expensive than their single-phase counterparts. This is why they are favored only in situations where single-phase systems are deemed incapable of meeting the cooling requirements of given device or system. Furthermore, the aforementioned advantages of convective phase change cooling are realized only within the nucleate boiling regime. This regime is maintained only as long as the coolant can adequately replenish the surface region where the liquid is rapidly converted to vapor. Intense vapor effusion ultimately begins to restrict liquid access to this region, triggering appreciable deterioration in the cooling effectiveness. This process reaches its most dangerous state at the critical heat flux (CHF), where the bulk liquid is no longer able to replenish the surface region. Should the device heat flux exceed this limit, most of the heat dissipated in the device will be trapped

* Corresponding author. Tel.: +1 765 494 5705; fax: +1 765 494 0539.
E-mail address: mudawar@ecn.purdue.edu (I. Mudawar).

0017-9310/$ - see front matter © 2006 Elsevier Ltd. All rights reserved.
doi:10.1016/j.ijheatmasstransfer.2006.01.008

Nomenclature

A_{ch}	portion of test surface area of unit cell dominated by channel flow
A_j	area of one slot jet
A_{jet}	portion of test surface area of unit cell dominated by jet impingement
A_t	test surface area
A_{total}	surface area of unit cell
c_p	specific heat at constant pressure
C_{sub}	empirical constant
d	characteristic length of flow boiling system
g	gravitational acceleration
H_{ch}	channel height
H_{gap}	Height of side channels
H_{jet}	jet height
h_{fg}	latent heat of vaporization
L	width of unit cell
L_{jet}	jet length
m	empirical constant
N	number of jets in flow distribution plate
n	empirical constant
P_W	electrical power supplied to copper block
Q	volumetric flow rate
q''_m	critical heat flux
q^{**}_m	dimensionless critical heat flux
T	temperature
T_f	liquid inlet temperature
T_s	average temperature of test surface
T_{sat}	saturation temperature
ΔT_{sub}	subcooling, $T_{sat} - T_f$
T_{tci}	temperature measured by thermocouple tc$i$ ($i = 1$–3)
U	mean jet velocity; characteristic velocity of flow boiling system
U_{ch}	channel velocity
W_{ch}	channel width
W_{jet}	jet width
W_w	half-width of wall separating channels
z	Cartesian coordinate

Greek symbols

μ	dynamic viscosity
ρ	density
σ	surface tension

Subscripts

ch	channel
exp	experimental
f	liquid
g	vapor
jet	impinging jet
m	maximum (critical heat flux)
pred	predicted
s	test surface
sat	saturation
sub	subcooling
tc$i$	thermocouple ($i = 1$–3)

in the device itself, causing a sudden unsteady escalation in the device temperature, which can lead to catastrophic failure. The ability to both predict and prevent CHF is therefore of paramount importance to the safety and integrity of any two-phase electronic cooling system.

Flow boiling CHF can be classified as either saturated or subcooled, depending upon the bulk fluid temperature at the outlet [2]. Saturated CHF is generally encountered with small flow rates, low inlet subcoolings and large length-to-diameter ratios; conditions where a significant fraction of the liquid flow is converted into a continuous vapor core. The remaining liquid is divided between a thin film that persists upon the heated wall and droplets that are entrained in the vapor core. Under these conditions, CHF takes the form of dryout of the liquid film. Micro-channel flows are especially prone to this type of CHF since they are used in applications demanding low flow rates and large length-to-diameter ratios [2].

Subcooled CHF is generally associated with high flow rates, small length-to-diameter ratios and high inlet subcoolings. Here, the bulk fluid maintains a predominantly liquid state at the outlet with a relatively small mass of vapor confined to the heated wall. Subcooling plays a vital role in all stages of the vaporization process. Subcooled liquid can absorb an appreciable fraction of the heat supplied at the wall before it is converted to vapor. This is why subcooled CHF can be far greater than saturated CHF for the same flow rate [3].

Decades of research have culminated in several useful correlations for CHF in both jet impingement and mini-/micro-channel flows. Most of these correlations are based on Katto's formulation for saturated flow boiling CHF, which provides a generic dimensionless form adaptable to different flow configurations, coolants, flow rates, and pressures [4].

$$\frac{q_{m,sat}/\rho_g h_{fg}}{U} = f\left[\frac{\rho_g}{\rho_f}, \frac{\rho_f U^2 d}{\sigma}, \frac{g(\rho_f - \rho_g)d}{\rho_f U^2}, \frac{\mu_g}{\mu_f}, \frac{\rho_f U d}{\mu_f}\right], \qquad (1)$$

where U and d are the characteristic velocity and characteristic length associated with the two-phase system. Additional dimensionless geometrical terms are also incorporated where the system involves more than one characteristic length. Observing a negligible dependence of experimental CHF data on viscosity or gravity, Katto suggested simplifying Eq. (1) to the following form:

$$\frac{q_{m,sat}/\rho_g h_{fg}}{U} = f\left[\frac{\rho_g}{\rho_f}, \frac{\rho_f U^2 d}{\sigma}\right]. \quad (2)$$

What is lacking in Eq. (2) is the strong dependence of CHF on subcooling. Mudawar et al. [5] and Mudawar and Maddox [6] modified an earlier theoretical CHF model that was developed by Haramura and Katto [7] for both pool boiling and flow boiling. The modified model incorporated the effects of subcooling on both the hydrodynamic instability between the liquid and vapor phases, and the energy required to vaporize the near-wall liquid just prior to CHF. They showed the ratio of subcooled to saturated CHF can be expressed as

$$\frac{q_m}{q_{m,sat}} = \left[1 + \frac{c_{p,f}\Delta T_{sub}}{h_{fg}}\right]^n \left[1 + C_{sub}\frac{\rho_f c_{p,f}\Delta T_{sub}}{\rho_g h_{fg}}\right]^m, \quad (3)$$

where C_{sub}, m, and n are empirical constants.

As discussed below, two flow configurations that are important to the present study are slot jets and micro-channel flow. Following is a brief discussion of CHF findings concerning these specific flows.

The vast majority of jet impingement studies concern single and multiple free circular jets. In one of the most comprehensive studies, Monde [8] identified different CHF regimes (V-, L-, I- and HP-regimes) for circular jets corresponding to different flow rates and different pressures. Monde and Mitsutake [9] extended these findings to multiple circular jets. Johns and Mudawar [10] showed the nozzle-to-surface distance has a negligible effect on CHF.

Mudawar and Wadsworth [11] developed a module that provided uniform cooling to a 3×3 array of heat sources, each cooled by a confined rectangular jet of FC-72. They developed a correlation for CHF independent of nozzle-to-surface distance and which showed CHF is proportional to $U^{0.7}$. A key practical finding from their study is that CHF is a far stronger function of jet velocity than flow rate. In other words, CHF can be increased for a fixed flow rate simply by decreasing the jet width. Recently, Meyer et al. [12] extended these findings to a heat source that is cooled by multiple slot jets.

Far fewer CHF studies are available for micro-channel heat sinks. Qu and Mudawar [2] recently examined CHF for a heat sink containing parallel rectangular micro-channels. They showed the interaction between micro-channels is responsible for drastic differences in CHF compared to a single micro-channel.

In recent years, the demand for more effective cooling solutions has spurred immense interest in the development of new innovative cooling schemes that capitalize upon the afore-mentioned merits of phase change. Of those, micro-channel flow and jet impingement are considered the two most effective solutions for devices demanding very high flux removal, such as high-performance microprocessors, laser diode arrays, and x-ray anodes [1]. This study explores the parametric trends of CHF for a new hybrid cooling scheme whose single-phase cooling performance was recently examined by the authors [13]. This scheme capitalizes upon the merits of both jet impingement and micro-channel flow. An area-averaged CHF correlation is constructed by applying CHF correlations for the portions of the heated surface that are influenced by jet impingement and channel flow.

2. Experimental methods

2.1. Test module

Fig. 1 shows the layered construction and assembly of the test module that housed the hybrid cooling device.

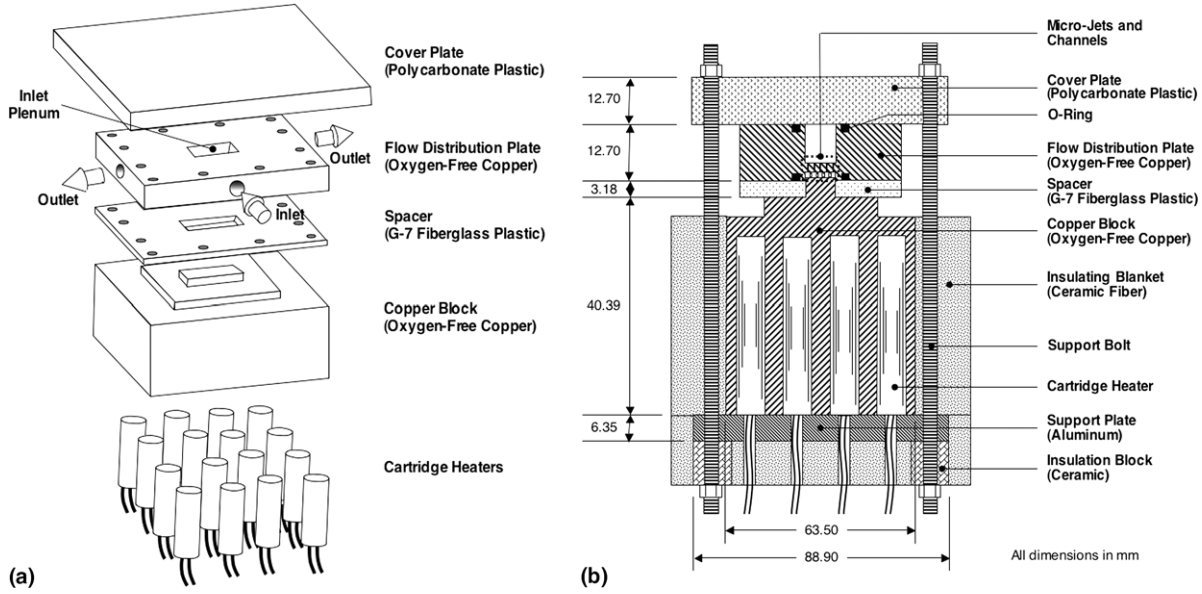

Fig. 1. (a) Test module construction. (b) Cross-section of module assembly.

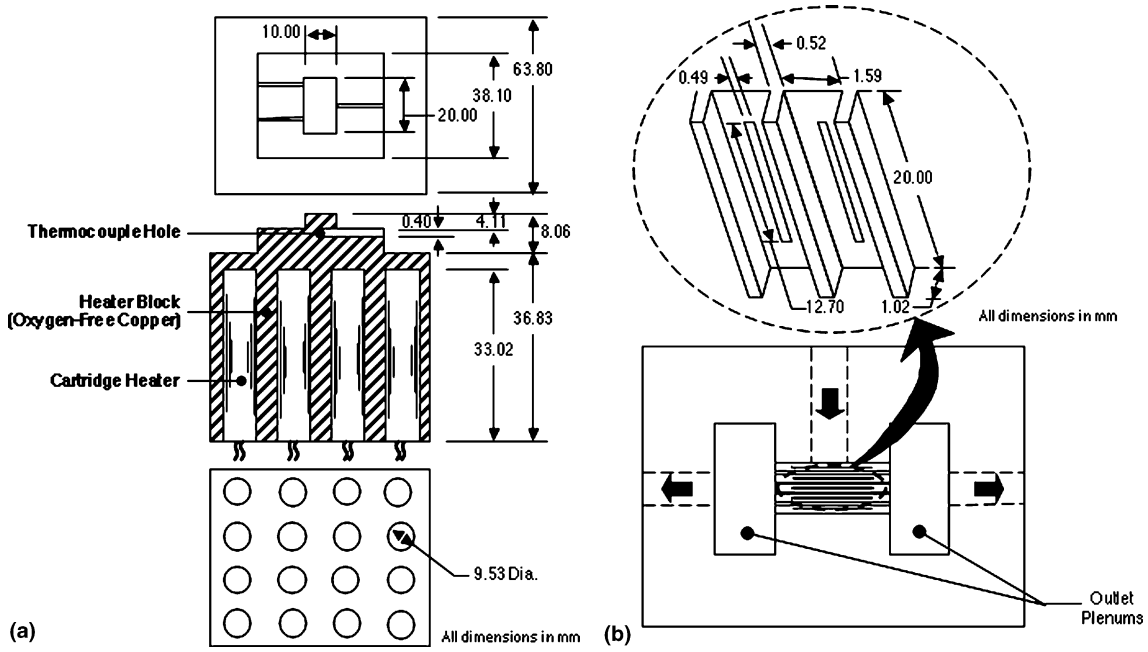

Fig. 2. Details of (a) heater block and (b) underside of flow distribution plate.

The test module consisted of a heater block, a flow distribution plate, a spacer, a cover plate, and 16 cartridge heaters. The copper heater block had a bulky underside where the cartridge heaters were inserted, and was stepped down into a uniform cross-sectional neck leading to the test surface. Three holes were drilled beneath the top surface to accommodate three chromel–alumel (K-type) thermocouples. Detailed dimensions of the heater block are given in Fig. 2(a).

All surfaces of the heater block save the top test surface were carefully insulated to minimize heat loss to the ambient. The neck portion was inserted into a spacer fabricated from high temperature fiberglass (G-7), while the outer surface of the lower bulky portion and underside were covered with ceramic blanket insulation and a solid ceramic plate, respectively.

Fig. 2(b) shows the flow distribution plate that included all the important features of the hybrid cooling configuration. The plate was machined from a single block of oxygen-free copper whose underside was grooved with five parallel 1.59 mm wide by 1.02 mm deep channels leading to two symmetrically opposite downstream plenums. Formed within each channel was a 0.48 mm wide, 0.76 mm deep, and 12.70 mm long slot jet. The flow distribution plate was covered on top with a polycarbonate plastic (Lexan) plate, forming an upstream plenum for the jets. Two o-ring seals prevented fluid leakage between the flow distribution plate and both the cover plate and the G-7 spacer.

Fig. 3(a) shows a schematic of a unit cell of the hybrid cooling configuration consisting of a single jet and a single channel. Fig. 3(b) shows key notations of the unit cell. A photo of underside of the flow distribution plate is given in Fig. 3(c). Key dimensions of the unit cell are given in Table 1.

2.2. Flow loop

Fig. 4 shows a schematic of a closed flow loop that was configured to deliver Fluorinert PF-5052 liquid at controlled pressure, temperature and flow rate into the test module housing the hybrid configuration. The coolant was circulated with the aid of a centrifugal magnetic drive pump. The flow rate was measured by one of two parallel rotameters having slightly overlapping flow rate ranges. An air-cooled heat exchanger brought the liquid to the desired module inlet temperature. The coolant flow was throttled with the aid of two control valves, one situated upstream and the other downstream of the test module. Aside from setting the flow rate, the upstream valve helped prevent a form of instability (pressure drop oscillation) that is commonly encountered in micro-channel heat sinks due to interaction between the two-phase flow in the heat sink itself and the flow loop's upstream compressible volume [2]. The downstream valve served mainly to set the desired outlet pressure.

The two-phase mixture exiting the test module was gravity-separated inside a large reservoir. Liquid from this reservoir drained directly into a second reservoir that served as a deaeration chamber, while the vapor was condensed by an air-cooled condenser situated atop the separation reservoir.

Before conducting any tests, the fluid was vigorously boiled for about 1 h by a cartridge heater in the loop's lower reservoir to purge any dissolved noncondensible

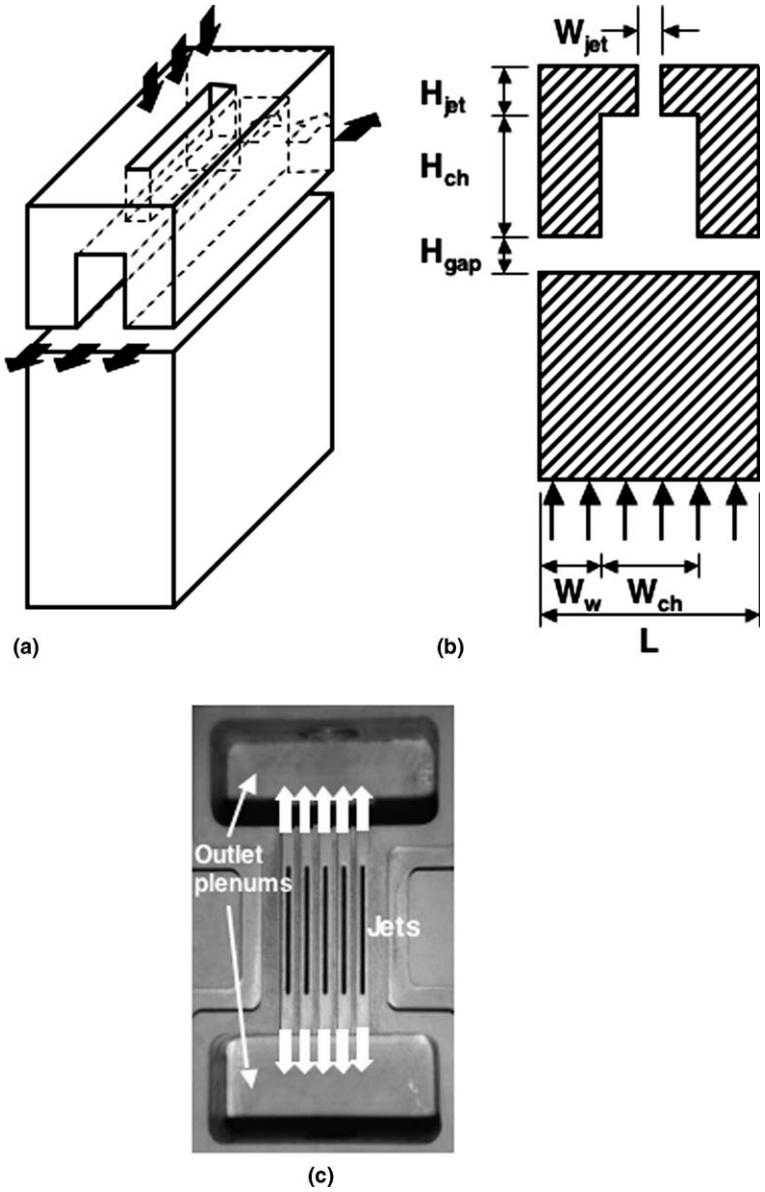

Fig. 3. (a) Schematic of unit cell consisting of single jet and single channel. (b) Impingement geometry for unit cell. (c) Photo of underside of flow distributor.

Table 1
Dimensions of unit cell of flow distribution plate

L_{jet} (mm)	W_{jet} (mm)	W_{ch} (mm)	W_w (mm)	H_{jet} (mm)	H_{ch} (mm)	H_{gap} (mm)
12.70	0.48	1.59	0.26	0.76	1.02	0.76

gases into the ambient. Afterwards, the loop components were adjusted to yield the desired module inlet conditions.

2.3. Data reduction

The total electrical power input to the 16 cartridge heaters was measured by a Yamaha WT 200 wattmeter. The heat flux, q'', from the test surface area of the heater block was calculated by dividing the total electrical power input, P_W, by the area of the test surface, $A_t = 1.0 \times 2.0\ \text{cm}^2$.

$$q'' = \frac{P_W}{A_t}. \tag{4}$$

The mean jet velocity was determined from the measured volumetric flow rate, Q, number of jets, N, and jet area, A_j.

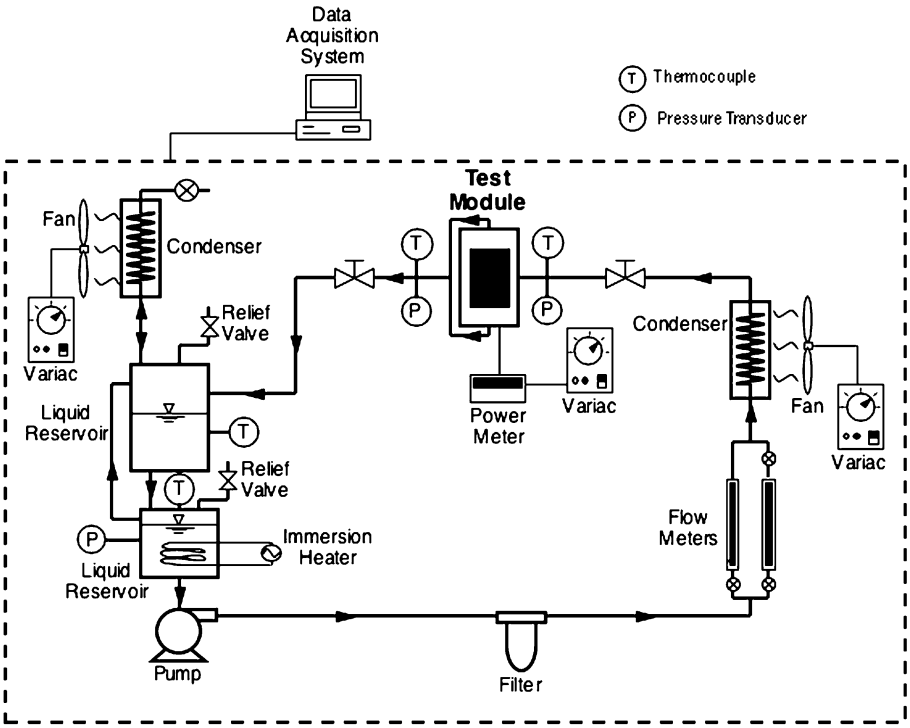

Fig. 4. Schematic of flow loop.

$$U = \frac{Q}{NA_j}. \tag{5}$$

CHF was detected by the thermocouple closest to the outlet in the form of a sudden unsteady temperature rise. The test was abruptly terminated to preclude physical damage to the test module materials. CHF was determined as the average of the prior surface heat flux and one-half the heat flux increment that precipitated the unsteady temperature rise. Using fine heat flux increments near CHF helped capture this event with high resolution.

Prior to performing the CHF measurement, a series of single-phase tests were conducted within the same flow rate range. Heat loss for the relatively low-power single-phase tests was estimated at less than 5% of the total electrical heat input, which decreased appreciably with increasing heat flux. Errors associated with the pressure transducer, rotameter, wattmeter, and thermocouple measurements were 0.5%, 1.0%, 0.5%, and 0.3 °C, respectively.

3. Results and discussion

3.1. Boiling curve trends

As indicated earlier, three thermocouples were inserted beneath the test surface to aid in determination of the surface temperature. These thermocouples were situated at distances of $z_{tc1} = 0.0$, $z_{tc2} = 5.0$, and $z_{tc3} = 7.5$ mm from the center of the flow channel. Fig. 5(a) and (b) shows boiling curves corresponding to the three thermocouple locations for a velocity of 2.15 m/s and inlet subcoolings of $\Delta T_{sub} = 13.1$ and 36.9 °C, respectively. The surface temperature, T_s, corresponding to each thermocouple was determined by correcting the thermocouple temperature for one-dimensional heat conduction between the thermocouple location and the test surface immediately above. The inlet temperature was measured directly by the thermocouple located upstream of the inlet plenum.

At low heat fluxes, the slopes of all boiling curves in Fig. 5(a) and (b) are constant, corresponding to the single-phase liquid cooling regime. With increasing heat flux, the slope of the boiling curve begins increasing at z_{tc3}, indicating boiling initiation near the outlet. This is consistent with the authors' numerical findings in a previous single-phase study of the present hybrid cooling configuration [13], which predicted highest surface temperatures at the channel outlet. A temperature offset among the three thermocouples is apparent along the single-phase and nucleate boiling regimes up to and including CHF. Notice the decreasing slope of the boiling curves prior to CHF, indicative of a deterioration in heat transfer effectiveness, which also begins at z_{tc3}. Eventually, CHF was detected at z_{tc3}. CHF values for the conditions given in Fig. 5(a) and (b) are 183.2 and 223.1 W/cm^2, respectively.

Figs. 6 and 7 show the effects of flow rate and subcooling, respectively, on the boiling characteristics. The surface temperature, T_s, in these plots was determined by area-averaging the surface temperatures extrapolated from the individual thermocouple measurements. Fig. 6 shows flow rate has a pronounced effect on all regimes of the boiling curve. Increasing flow rate augments the single-phase heat transfer considerably and delays the point of boiling

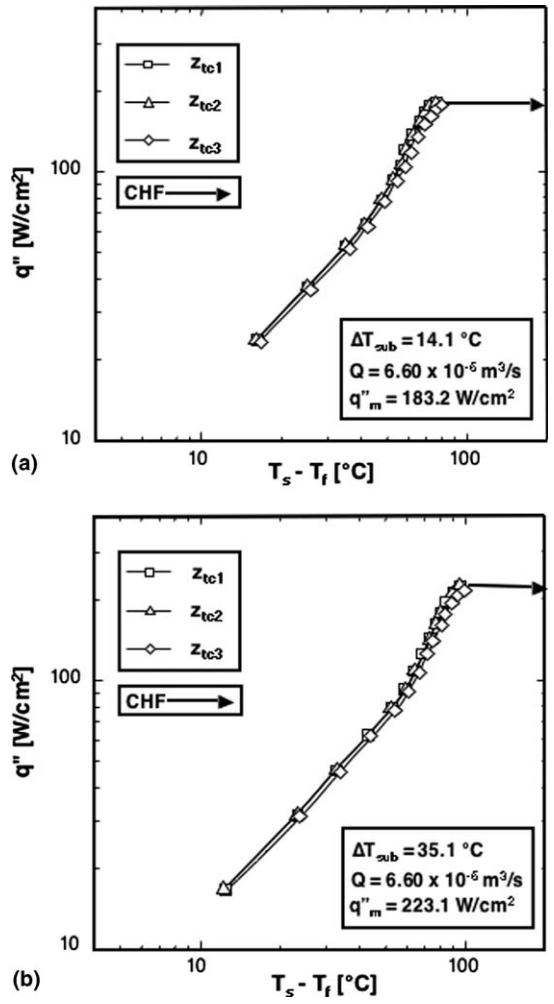

Fig. 5. Boiling curves measured at z_{tc1}, z_{tc2} and z_{tc3} for (a) $\Delta T_{sub} = 14.1$ °C and $Q = 6.60 \times 10^{-5}$ m^3/s and (b) $\Delta T_{sub} = 35.1$ °C and $Q = 6.60 \times 10^{-5}$ m^3/s.

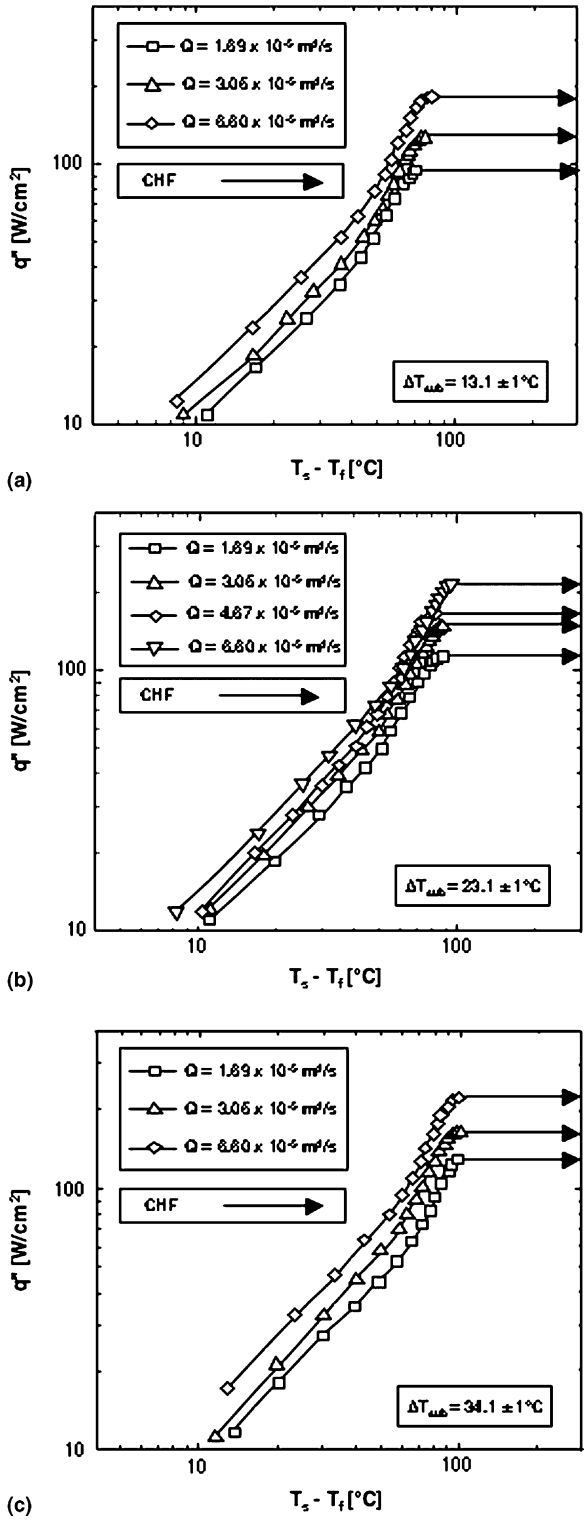

Fig. 6. Flow rate effects on boiling curve for (a) $\Delta T_{sub} = 13.1 \pm 1$ °C, (b) $\Delta T_{sub} = 23.1 \pm 1$°C, and (c) $\Delta T_{sub} = 34.1 \pm 1$ °C.

incipience to a higher heat flux and a higher surface temperature. Increasing flow rate also increases CHF appreciably.

Fig. 7 captures the effects of subcooling on the boiling curve. These effects are minimal in the single-phase regime, where the convective heat transfer coefficient is only slightly altered by coolant property variations with temperature. However, there is a noticeable effect of subcooling on the point of boiling incipience, where both heat flux and surface temperature increase with increasing subcooling. Fig. 7 also shows a significant enhancement in CHF with increased subcooling.

Fig. 8 shows CHF variations with volumetric flow rate for different inlet subcoolings. As depicted earlier in Figs. 6 and 7, increases in inlet subcooling and/or flow rate serve to increase CHF.

3.2. Assessment of previous CHF correlations

Mudawar and Wadsworth [11] surveyed previous CHF studies concerning flow over small heated surfaces including circular impingement jets, free wall jets, confined wall jets and channel flow to explain the CHF dependence on flow velocity for confined slot jet impingement. They concluded that confining the flow following impingement serves to enhance liquid access to the test surface, evidenced by a greater CHF and a stronger dependence of CHF on jet velocity compared to a free jet.

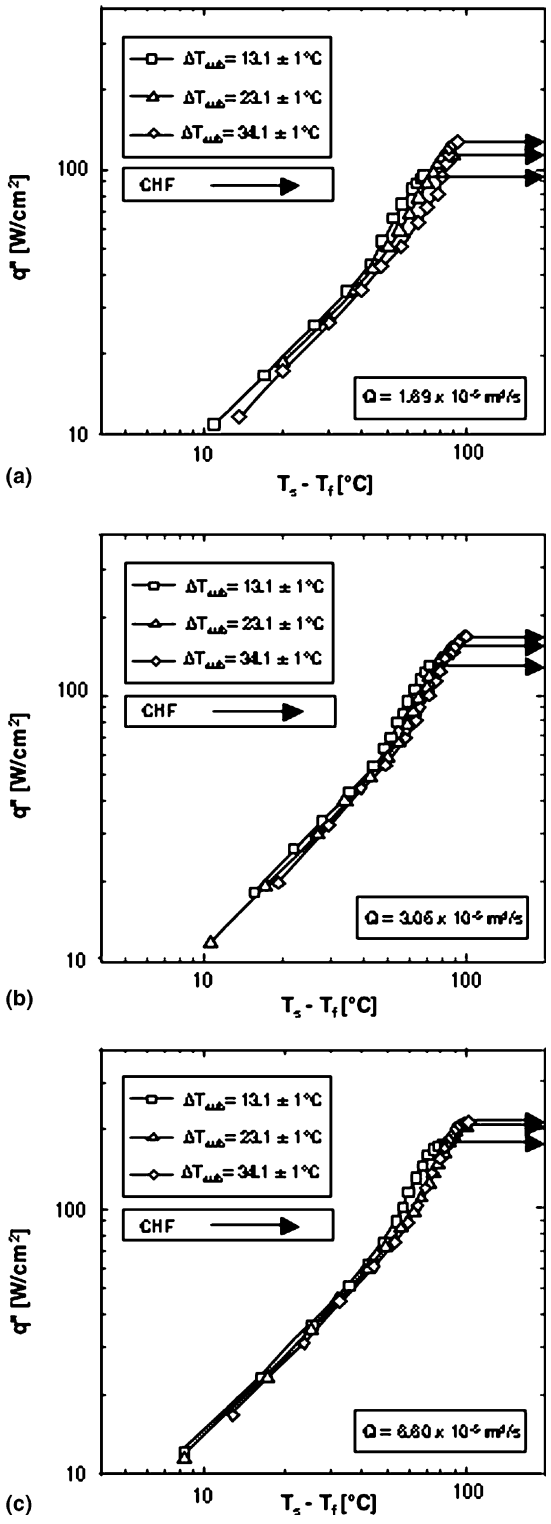

Fig. 7. Subcooling effects on boiling curve for (a) $Q = 1.69 \times 10^{-5}$ m^3/s, (b) $Q = 3.05 \times 10^{-5}$ m^3/s, and (c) $Q = 6.60 \times 10^{-5}$ m^3/s.

Interestingly, Fig. 8 shows a CHF dependence for the present hybrid cooling configuration of $q''_m \propto U^{0.45}$. This velocity exponent is between that for channel flow, $q''_m \propto U^{0.30}$ [6], and confined slot jet impingement, $q''_m \propto U^{0.70}$ [11]. This can be explained by the present configuration being a hybrid of slot jet impingement and channel flow.

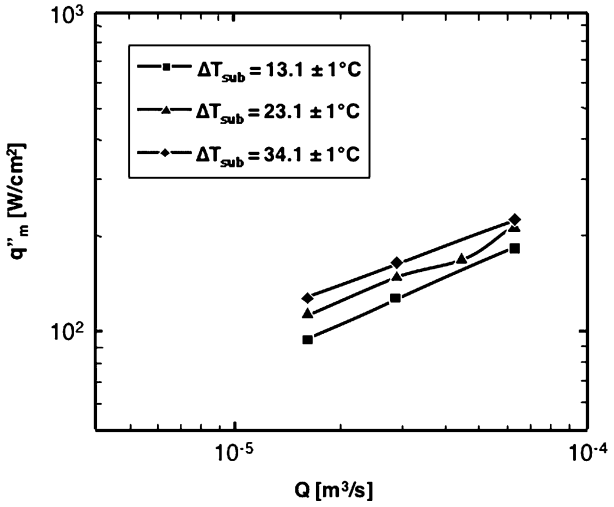

Fig. 8. Variation of CHF with flow rate for three subcoolings.

Table 2
Correlations for subcooling flow boiling CHF

Authors	Correlations
Mudawar and Maddox [6]	Channel flow: $q''^{*}_{m} = \frac{\frac{q''_m}{\rho_g h_{fg} U_{ch}}}{\left(\frac{\rho_f}{\rho_g}\right)^{15/23}\left(\frac{L}{D}\right)^{7/23}\left(1+0.021\frac{\rho_f c_{p,f}\Delta T_{sub}}{\rho_g h_{fg}}\right)^{16/23}\left(1+\frac{c_{p,f}\Delta T_{sub}}{h_{fg}}\right)^{7/23}} = 0.161\left(\frac{\sigma}{\rho_f U_{ch}^2 L}\right)^{8/23}$
Mudawar and Wadsworth [11]	Confined slot jet: $q''^{*}_{m} = \frac{\frac{q''_m}{\rho_g h_{fg} U}}{\left(\frac{\rho_f}{\rho_g}\right)^{2/3}\left(\frac{W}{L-W}\right)^{0.396}\left(1+0.058\frac{\rho_f c_{p,f}\Delta T_{sub}}{\rho_g h_{fg}}\right)^{2/3}\left(1+\frac{c_{p,f}\Delta T_{sub}}{h_{fg}}\right)^{1/3}} = 0.0786\left(\frac{\sigma}{\rho_f U^2 (L-W)}\right)^{149}$
Meyer et al. [12]	Multiple confined slot jets: $q''^{*}_{m} = \frac{\frac{q''_m}{\rho_g h_{fg} U}}{\left(\frac{\rho_f}{\rho_g}\right)^{2/3}\left(1+0.034\frac{\rho_f c_{p,f}\Delta T_{sub}}{\rho_g h_{fg}}\right)^{2/3}\left(1+\frac{c_{p,f}\Delta T_{sub}}{h_{fg}}\right)^{1/3}\left(\frac{W}{L-W}\right)^{0.331}} = 0.0919\left(\frac{\sigma}{\rho_f U^2 (L-W)}\right)^{0.157}$

To further explore this relationship, predictions of a previous CHF correlation for channel flow [6] and two correlations for slot jet impingement [11,12] were examined for accuracy in predicting CHF data for the present hybrid cooling configuration. These correlations are given in Table 2. The accuracy of the predictions is based on mean absolute error (MAE), which is defined as

$$\mathrm{MAE} = \frac{1}{M}\left(\sum \frac{|q''_{m,\mathrm{pred}} - q''_{m,\mathrm{exp}}|}{q''_{m,\mathrm{exp}}} \times 100\%\right). \quad (6)$$

First, the predictions of a given correlation are applied along the entire test surface. Fig. 9(a) shows the Mudawar and Maddox channel flow correlation underpredicts the present CHF data with a MAE of 53.89%. This shows the hybrid configuration yields CHF values appreciably higher than those of channel flow.

Fig. 9(b) and (c) compares predictions of the Mudawar and Wadsworth correlation and the Meyer et al. correla-

tion with the present CHF data. While the first correlation was developed for FC-72 and single slot jets, the latter was validated for both FC-72 and ethyl alcohol, as well as multiple slot jets. Both correlations provide reasonable predictions, with MAEs of 14.20% and 11.48%, respectively, and most of the data points falling within a ±20% error band. The success of these correlations points to jet impingement dominating cooling behavior inside the present hybrid cooling scheme. Nonetheless, the basis for this comparison is somewhat questionable since jet impingement is confined to only a portion of the test surface. A more systematic approach to correlating CHF data is therefore required.

3.3. New CHF correlation scheme

In this section, a new CHF correlation approach is developed that is specifically tailored to hybrid configurations having different cooling mechanisms dominating different portions of a test surface.

Previous numerical findings by the present authors concerning the single-phase cooling performance of the present hybrid cooling scheme have shown the jet flow produces a

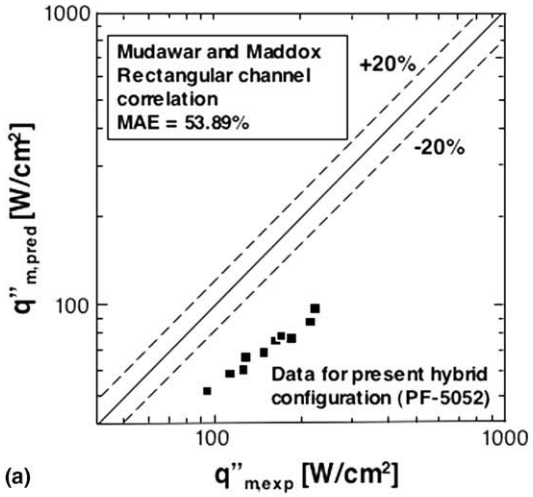

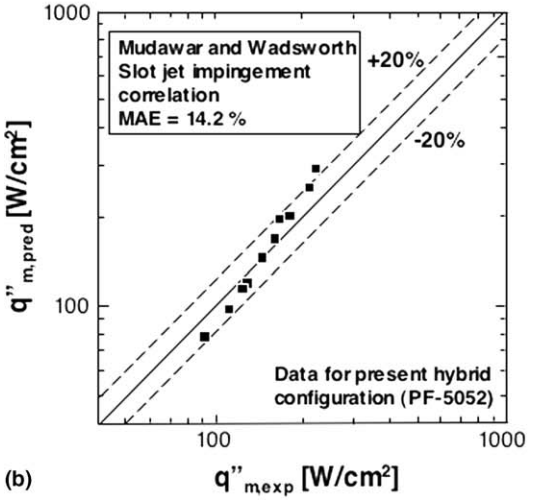

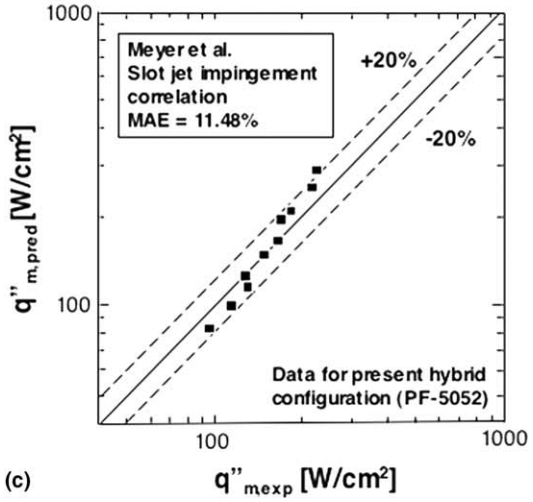

Fig. 9. Comparison of CHF data for PF-5052 in present hybrid configuration with predictions of (a) channel flow correlation of Mudawar and Maddox, (b) single slot jet correlation of Mudawar and Wadsworth, and (c) multiple slot jet correlation of Meyer et al.

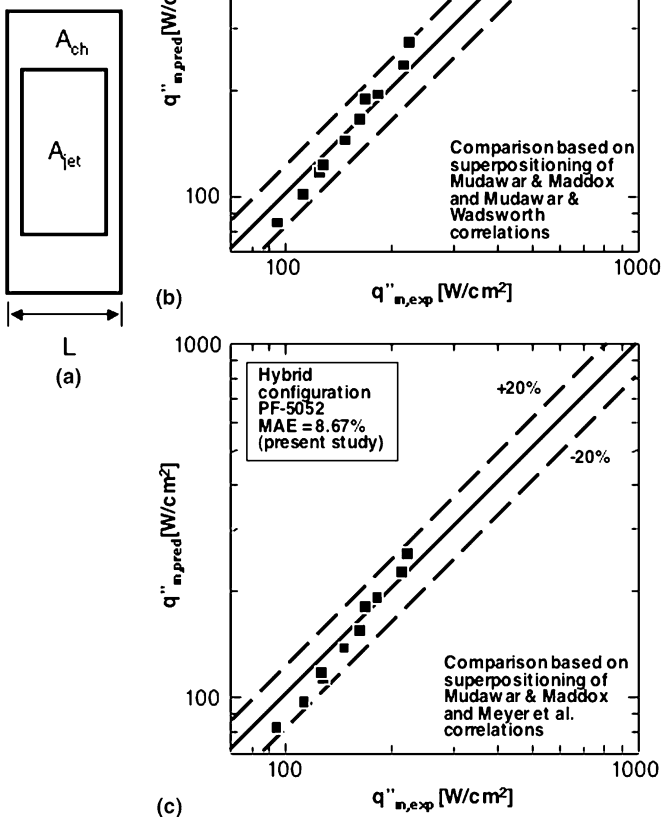

Fig. 10. (a) Superpositioning of channel flow and jet impingement portions of unit cell. Comparison of CHF data for PF-5052 in present hybrid configuration with predictions based on superpositioning (b) Mudawar and Maddox and Mudawar and Wadsworth correlations, and (c) Mudawar and Maddox and Meyer et al. correlations.

strong vorticity effect confined to the width, W_{ch}, of the flow channel [13]. This indicates jet impingement is dominant over this region of the test surface. A slot jet correlation (Mudawar and Wadsworth or Meyer et al.) was therefore applied over an effective impingement area of $A_{jet} = W_{jet}L_{jet}$ of the unit cell illustrated in Fig. 3(b), while the Mudawar and Maddox channel flow correlation was adopted for a channel flow area of $A_{ch} = A_{total} - A_{jet}$. Fig. 10(a) illustrates this superpositioning scheme. The CHF correlation for the hybrid cooling configuration is defined as

$$q''_m A_{total} = q''_{m,jet} A_{jet} + q''_{m,ch}(A_{total} - A_{jet}), \quad (7)$$

where $q''_{m,jet}$ and $q''_{m,ch}$ are the CHF values predicted by the slot jet correlation and the Mudawar and Maddox correlation, respectively.

Fig. 10(b) compares predictions of the new CHF correlation scheme with the present CHF data using the slot jet correlation of Mudawar and Wadsworth over A_{jet}. An overall MAE of 8.42% clearly demonstrates the excellent predictive capability for the hybrid configuration. The same superpositioning scheme is attempted in Fig. 10(c) by applying the Meyer et al. correlation over A_{jet}. While the MAE error for this case (8.67%) is slightly higher, it appears almost equally effective at predicting the CHF data using the new superpositioning technique.

4. Conclusions

This study examined the two-phase heat transfer performance of a new hybrid cooling scheme combining the cooling attributes of slot jets and micro-channel flow. A test module was constructed and tested using Fluorinert PF-5052 to explore both the boiling trends and CHF characteristics. Previous CHF correlations for channel flow and jet impingement were examined for suitability to predicting data for the hybrid cooling configuration. A new correlation scheme was devised to more accurately correlate the CHF data. Key findings from the study are as follows:

1. Increasing flow rate both increases the single-phase heat transfer coefficient and delays the inception of boiling. Increasing subcooling has a weak effect on the single-phase region but delays both the heat flux and surface temperature corresponding to incipient boiling.
2. CHF occurs first at the downstream edge of the test surface. Like most flow boiling systems, higher CHF values are realized with the hybrid cooling configuration with increases in flow rate and/or subcooling.
3. A previous channel flow CHF correlation predicts values far smaller than measured, while those for slot jets yield closer predictions. This proves the cooling performance of the hybrid configuration is dominated more by jet impingement than by channel flow.
4. A new simple CHF correlation scheme is devised which incorporates predictions of channel flow and slot jet impingement over the portions of the test surface dominated by each flow pattern. An overall MEA of 8.42% demonstrates the accuracy of this correlation scheme at predicting data for the hybrid configuration.

Acknowledgement

The authors are grateful for the support of the Office of Naval Research (ONR) for this research.

References

[1] I. Mudawar, Assessment of high-heat-flux thermal management schemes, IEEE Trans.—Components Packaging Tech. 24 (2001) 122–141.
[2] W. Qu, I. Mudawar, Measurement and correlation of critical heat flux in two-phase micro-channel heat sinks, Int. J. Heat Mass Transfer 45 (2002) 2549–2565.
[3] J.G. Collier, J.R. Thome, Convective Boiling and Condensation, third ed., Oxford University Press, Oxford, 1994.
[4] Y. Katto, Critical heat flux in forced convective flow, in: Proc. ASME/JSME Thermal Engng. Joint Conf., Hawaii, vol. 3, 1983, pp. 1–10.
[5] I. Mudawar, T.A. Incropera, F.P. Incropera, Boiling heat transfer and critical heat flux in liquid films falling on vertically-mounted heat sources, Int. J. Heat Mass Transfer 30 (1987) 2083–2095.
[6] I. Mudawar, D.E. Maddox, Critical heat flux in subcooled flow boiling of fluorocarbon liquid on a simulated electronic chip in a vertical rectangular channel, Int. J. Heat Mass Transfer 32 (1989) 379–394.
[7] Y. Haramura, Y. Katto, A new hydrodynamic model of critical heat flux applicable to both pool and forced convection boiling on submerged bodies in saturated liquids, Int. J. Heat Mass Transfer 26 (1983) 389–399.
[8] M. Monde, Critical heat flux in saturated forced convection boiling on a heated disk with an impinging jet, ASME J. Heat Transfer 109 (1987) 991–996.
[9] M. Monde, Y. Mitsutake, Critical heat flux in forced convective subcooled boiling with multiple impinging jets, ASME J. Heat Transfer 117 (1996) 241–243.
[10] M.E. Johns, I. Mudawar, An ultra-high power two-phase jet-impingement avionic clamshell module, ASME J. Electron. Packaging 118 (1996) 264–270.
[11] I. Mudawar, D.C. Wadsworth, Critical heat flux from a simulated chip to a confined rectangular impinging jet of dielectric liquid, Int. J. Heat Mass Transfer 34 (1991) 1465–1479.
[12] M.T. Meyer, I. Mudawar, C.E. Boyack, C.A. Hale, Single-phase and two-phase cooling with an array of rectangular jets, Int. J. Heat Mass Transfer 49 (2006) 17–29.
[13] M.K. Sung, I. Mudawar, Experimental and numerical investigation of single-phase heat transfer using a hybrid jet impingement/micro-channel cooling scheme, Int. J. Heat Mass Transfer 49 (2006) 682–694.